e+i elektrotechnik und informationstechnik

Open-source design of integrated circuits

An open-sourced 1.44-MS/s 703-μW 12-bit non-binary SAR-ADC using 448-aF capacitors in 130-nm CMOS

Patrick Fath (ID) · **Manuel Moser** · **Georg Zachl** · **Harald Pretl** (ID)

Abstract This paper presents the design of a self-clocked 12-bit non-binary fully differential SAR-ADC using the SKY130 open-source PDK. The entire mixed-signal circuit design and layout were created with free and open-source software. The ADC reaches a sample rate of up to 1.44 MS/s at 1.8 V supply while consuming 703 μW of power on a small 0.175 mm^2 area. A configurable decimation filter can increase the ADC resolution up to 16 bits while using an oversampling factor of 256. A 9-bit thermometer-coded and 3-bit binary-coded DAC matrix using a 448 aF waffle-capacitor results in a total capacitance of 1.83 pF per input. Realizations of configurable analog functions using the form factor of SKY130 high-density standard cells allow the parametrization of an analog circuit in a hardware description language and hardening of the macro in an intentionally digital workflow.

Keywords Charge redistribution DAC · CMOS · Digital-friendly · EDA · FOSS · Integrated circuit · Low power · Open source · OSIC · RTL-to-GDS · SAR-ADC · SKY130 · Top level hardening

Einsatz freier und quelloffener Software für den Entwurf integrierter Schaltungen
Ein quelloffener 1,44-MS/s 703-μW 12-bit nichtbinärer SAR-ADC mit 448-aF Kondensatoren in einem 130-nm CMOS-Prozess

Zusammenfassung Dieses Manuskript beschreibt das Design eines selbsttaktenden, volldifferenziellen, nichtbinären 12-Bit SAR-ADC, welcher für die SKY130-Technologie mit einem Open Source-PDK entwickelt wurde. Das Schaltungsdesign bis hin zum produktionsfertigen Layout wurde ausschließlich mit freier Open Source-Software erstellt. Der ADC erreicht eine Abtastrate von bis zu 1,44 MS/s bei einer Versorgungsspannung von 1,8 V. Die Leistungsaufnahme liegt dabei bei 703 μW. Der komplette SAR-ADC mit allen zugehörigen Schaltungskomponenten nutzt 0,175 mm^2 Fläche. Mittels eines konfigurierbaren, digitalen Dezimierungsfilters mit einer maximalen Überabtastrate von 256 kann die Auflösung des SAR-ADCs auf bis zu 16 Bit erhöht werden. Der SAR-ADC nutzt eine 12-Bit DAC-Matrix, welche in 9-Bit Thermometer- und 3-Bit binär-codierte Zellen aufgeteilt ist. Um eine möglichst gute Übereinstimmung der Zellen zu erreichen, wird die gesamte Matrix aus Einheitskondensatoren mit einer Kapazität von 448 aF aufgebaut. Dies ergibt eine Gesamtkapazität von 1,83 pF pro Eingang. Um den manuellen Design-Aufwand zu minimieren, wurde ein Teil der analogen Schaltung mittels eines digitalen Designablaufes realisiert. Dabei wurden zusätzliche Zellen im Formfaktor von digitalen Standardzellen der Technologie entwickelt. Damit können nun analoge Komponenten ohne zusätzliche Intervention vollautomatisch parametrisiert und bis zum fertigen Layout entworfen werden.

Schlüsselwörter CMOS · Digital-friendly · EDA · FOSS · Integrierte Schaltung · Ladungsumverteilungs-DAC · OSIC · Quelloffen · RTL-zu-GDS · SAR-ADC · SKY130 · stromsparend · Top Level-Hardening

1 Introduction to open-source IC design

Free and open-source software (FOSS) for the design of integrated circuits (IC) has been around for decades. The most prominent specimen, the Simulation Program with Integrated Circuit Emphasis

P. Fath (✉) · M. Moser · G. Zachl · H. Pretl
Institute for Integrated Circuits, Johannes Kepler University
Linz, Altenberger Straße 69, 4040 Linz, Austria
patrick.fath@jku.at

Table 1 Open-Source tools and PDK available in IIC-OSIC-TOOLS used in this ADC

Tool	Usage	Ref.
Xschem	Graphical schematic entry tool for full-custom circuit design incl. waveform viewer	[29]
ngspice	SPICE-level mixed-mode (analog plus digital) circuit simulator	[21]
Xyce	High-performance SPICE-level analog circuit simulator with support for large-scale parallel computing	[42]
Magic	Custom layout editor supporting DRC and parasitic extraction	[9, 25]
KLayout	Fast custom layout editor with DRC and LVS support	[15]
netgen	Netlist comparison tool used for LVS	[10]
osic-multitool	User scripts for DRC, LVS, parasitic extraction (PEX), Verilog linting, etc.	[26]
Icarus Verilog	Digital simulator and linter for Verilog	[38]
Verilator	High-performance digital simulator and linter for Verilog	[36]
Yosys	Digital synthesis tool for Verilog	[39, 40]
OpenLane	RTL-to-GDS flow (control and configuration scripts)	[23, 33]
OpenROAD	RTL-to-GDS engine: automatic placement and routing, delay extraction, and static timing analysis	[1, 2, 24]
SKY130	SkyWater Technologies 130-nm CMOS open-source PDK	[34]

(SPICE), was one of the first simulators for electronic circuits in widespread use and is still the foundation for most of today's commercial and FOSS simulators. Since then, FOSS for IC design has been a marginal phenomenon, that was mostly relevant for academic research.

Recently, FOSS for IC design has experienced a renaissance, with efforts of companies like Alphabet (Google) and a considerable community of enthusiasts from academia and hobbyists, as well as commercial entities trying to simplify the access and usage of a stack of tools for digital and analog design. Sponsored or low-cost multi-project wafer runs allow private individuals, low-budget academic research, and startup companies to enter IC design, explore new creative ideas, and lower the entrance barrier to this otherwise budget-intensive topic.

All these advances have led to a new spark in the FOSS IC design area, which continuously picks up pace. Multiple complete RTL-to-GDS flows for digital design are available, combining many tools, and the tools for analog design are also maturing. Finally, two open-source Process Design Kits (PDK) (and more are announced) allow everyone to access the information required to design a chip.

Besides the benefit in IC research and development of easily shareable designs and results in scientific papers (like publishing the full design files of a circuit together with the usual measurement results), these open-source EDA stacks allow the use in teaching without the necessity of SW licenses, PDK NDAs, and the mandatory (but hindering) access restrictions for IP protection.

2 Open-source IC design software stack and usage

The usage of open-source software in the construction of IC is not just a recent phenomenon. Quite the contrary, many important developments in the IC area started at university research labs many years ago, and the resulting software has been made pub-

licly available under open-source licenses. The venerable SPICE [20] or the layout editing tool Magic [25] are just two examples (and interestingly, both are still in use today).

Furthermore, freely available open-source PDKs are not a recent development either, with examples like ASAP7 [7] being quite well-known and often used in research papers. However, the (until recently) available PDKs like ASAP7 are *theoretical* PDKs, which means that (at best) simulation data can be created and a layout file (GDS) can be produced, but no IC can be actually manufactured from these efforts.

This situation changed drastically in 2020 when SkyWater Technologies and Google released the first open-source *manufacturable* PDK [41]. This swung open the door to the possibility of having an actual IC manufactured in a mature node (130 nm), designed exclusively with open-source design tools, and with access to a PDK and process documentation without the need for signing a non-disclosure agreement (NDA).

However, one caveat is that to arrive at a fully functional design flow, many SW packages must be downloaded, locally compiled, package dependencies resolved, configurations set correctly, and so on—all this without a professional support hotline. While it is known that electronic design automation (EDA) flows for IC are complex, this additional layer of difficulty is a significant entry barrier for newcomers. To substantially lower this barrier, packaged, configured, and tested environments like the IIC-OSIC-TOOLS [27] are available; this SW stack has also been used in the development of this ADC.[1]

---

[1] For ease of use, the OS-level virtualization environment Docker [8] is used for the IIC-OSIC-TOOLS. The ready-made Docker container contains the base OS and all SW-dependencies, allowing good performance of this virtual machine when run on a wide range of host machines and host operating systems, like Windows, Linux, and macOS. The virtual machine can be accessed via various modes like VNC, Jupyter notebook, or even a simple web browser, running locally or on a remote server.

Table 1 lists the used SW components of this environment for the presented mixed-signal design, while many more are available, as documented in the README of [27]. As can be seen, a full custom (analog) design flow is supported spanning from circuit entry, via simulation, to layout design and parasitic extraction. Likewise, a digital RTL-to-GDS flow is supported using OpenLane/OpenROAD [2, 33], which allows the effective implementation of large digital circuits [11].

Fig. 1 depicts how the individual building blocks are constructed and assembled into the final top-level block. Custom analog blocks like the capacitor matrix, comparator, and the V_{CM}-generating charge pump consist of a schematic SPICE netlist (used for simulation and LVS), which is created using Xschem and a layout view created in Magic. Magic can also write an LEF- and a GDS-file, which, together with a Verilog stub, is used for top-level assembly using OpenLane/OpenROAD.

With the same tool set, custom digital standard cells can also be created, which has been used for creating dedicated large-delay cells, as the available delay cells in the SKY130 libraries proved inadequate for this design. Behavioral Verilog models are synthesized and tech-mapped into a SKY130 gate-level representation using Yosys [40], and all subcomponents (custom analog, custom digital, and standard digital) are automatically placed and routed using OpenLane/OpenROAD, requiring only minimal manual intervention.

3 Circuit design

As shown in Fig. 2, the presented SAR-ADC consists of segmented capacitive digital-to-analog converters (DAC), a self-clocking mechanism, an embedded switched-capacitor voltage divider for common-mode voltage generation, a fully dynamic two-stage latch comparator as proposed in [12] and a digital control block with an integrated oversampling decimation filter. However, this paper focuses on the DAC, the self-clocking mechanism, and the digital control block.

The internal clock generation is based on custom-designed delay cells in the form factor of a SKY130 digital standard cell. This allows the parametrization of an analog circuit in a hardware description language (HDL) and hardening using an unmodified digital design workflow.

The proposed SAR-ADC has a physical resolution of 12 Bit, which can be increased up to 16 Bit by oversampling followed by a boxcar decimation filter with a selectable oversampling rate (OSR) up to 256. The four least significant SAR weights include a digital averaging filter to reduce the sampled noise. Post-layout simulations reveal a maximum sampling rate of 1.44 MS/s with nominal process parameters. Sources, schematics, and the final layout are published on GitHub [18] within the Apache-2.0 license.
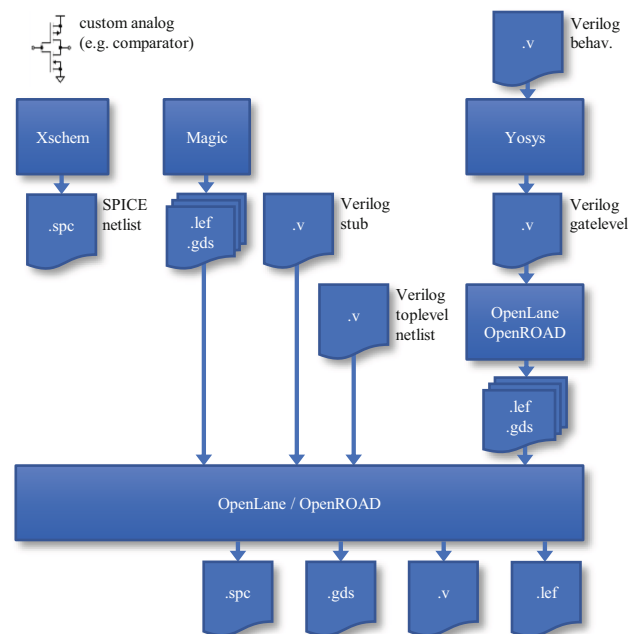

Fig. 1 Block diagram of the proposed open-source design flow, including the essential tools and used/generated files

3.1 Digital-to-analog converter (DAC) matrix

Due to its simplicity and power efficiency, a 12-bit digital-to-analog converter based on charge-redistribution [37] is used for the proposed SAR-ADC. In this case, the input signal is sampled onto a capacitive array using the top-plate sampling method. As shown in Fig. 3, the DAC matrix is segmented into 511 cells of a 9-bit thermometer code and three cells of a 3-bit binary code [16] for area-efficiency and improved linearity. In addition, an arrangement of the whole DAC matrix with fairly equal capacitor cells reduces offset and mismatch errors. A single thermometer cell consists of $8C$ unit capacitors (whereas $C^0 = 447\,\text{aF}$) in an area of $25\,\mu\text{m}^2$. The binary cells are constructed from a thermometer cell with binary weighted unit capacitors of $1C/2C/4C$.

3.1.1 Layer stack considerations

The number and properties of available routing layers in the SKY130 layer stack [35] must be considered in the early phase of system-level planning. The SKY130 PDK is limited to one local-interconnect-layer li and 5 metal routing-layers m1–m5. Since the design rules were disadvantageous for an area-efficient design using layer m5, it was fully dedicated to the top-level power distribution network (PDN). In this case, layers m2, m3, and m4 are used for the capacitor layout.

Since the capacitor is realized using metal layers m2–4, the routing of the decoder circuit as shown in Fig. 6 must be done in the residual layers li and m1. Using the local interconnect layer for routing is a compromise to allow the waffle capacitor design on top of the decoder to use three metal layers for best match-

ing performance, but the higher sheet resistance of $R_{s,li} = 12.8\,\Omega/\square$ (in comparison to metal layers) could become the limiting factor regarding DAC speed.
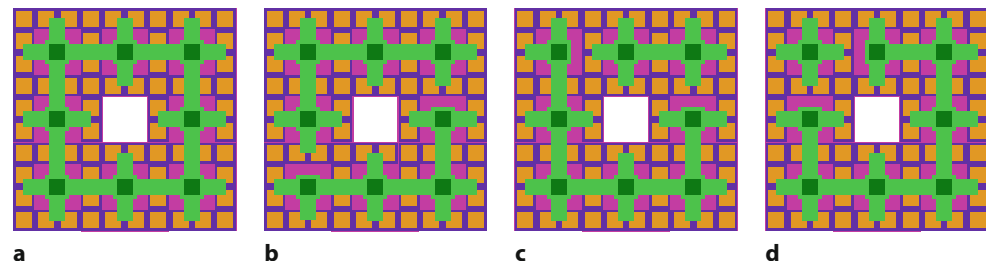
3.1.2 Capacitor topology evaluation

For evaluation of matching and capacitance values in different types of thermometer- and binary-code capacitors, eight different finger- and waffle-capacitor structures, as shown in Fig. 5, were compared with a focus on matching, capacitance, and area. Table 2 shows the cell capacitance C_{cell} and the unit cap capacitance of the resulting binary cells C^0_{1-16}. Structures a and b of Fig. 5 show the most suitable compromise concerning matching, capacitance density, and

Fig. 5 Layouts of the investigated capacitor topologies. Topology **a** and **b** are waffle-capacitor based, **d–h** are inspired by finger-capacitors, and **c** is a hybrid of both structures. The main capacitance of structures **a–d, g** is in layer m3-m3, structures **e** and **f** use m3-m4 while the main capacitance of **h** is located in m4-m4 [19]
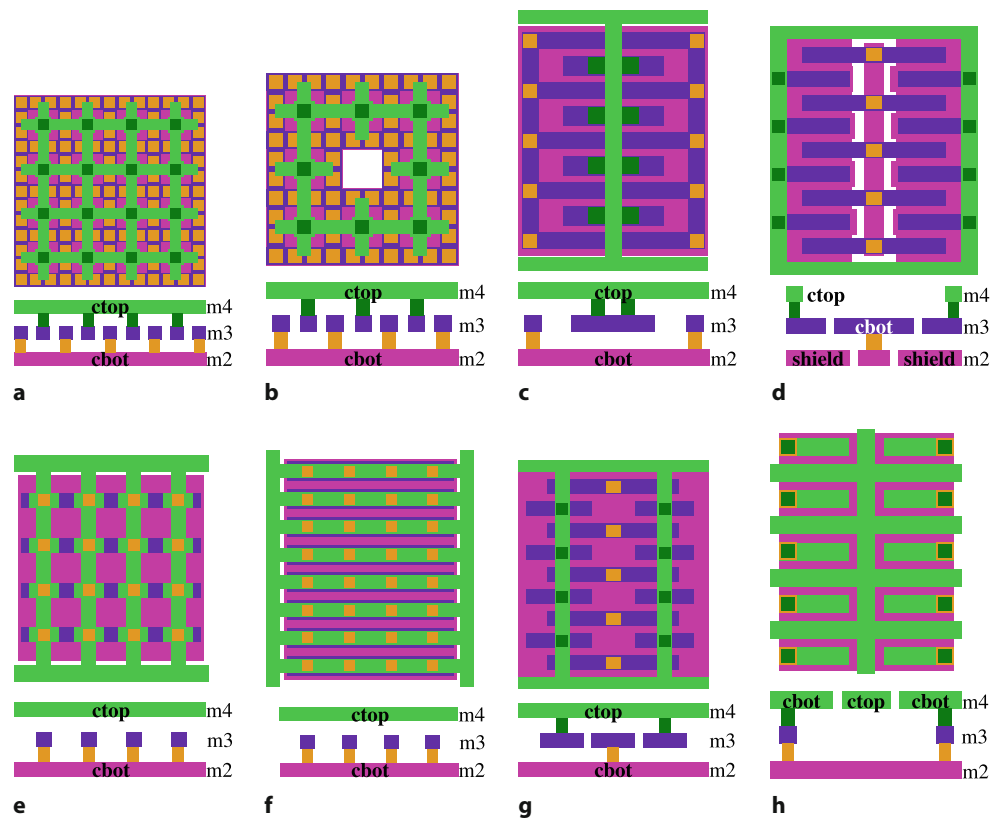

Fig. 6 Schematic of the DAC drive cell complementary sample signal generator [28] and the row/column decoder circuit [31], which are both integrated into the DAC cells
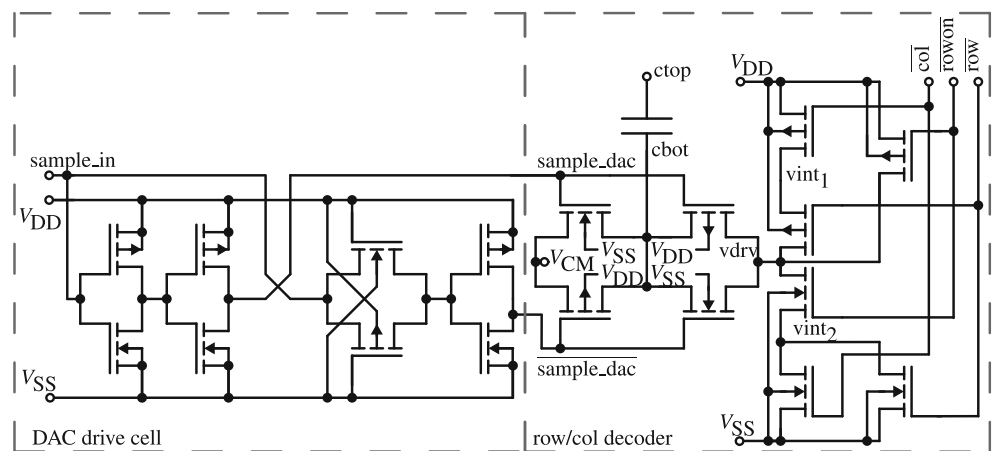

Table 2 Extracted capacitance values of the investigated topologies

Capacitor in Fig. 5	(a)	(b)	(c)	(d)	(e)	(f)	(g)	(h)
Unit caps C^0 per cell	16	8	8	8	16	8	8	8
Area per cell (µm²)	41	25	23	22	17	24	28	19
Cell cap C_{cell} (fF)	9.2	4.8	0.6	3.1	0.7	1.1	5.6	5.0
Unit cap C_{16}^0 (aF)	572	–	–	–	46	–	–	–
Unit cap C_8^0 (aF)	595	593	76	389	51	134	695	621
Unit cap C_4^0 (aF)	637	620	–	385	75	173	705	672
Unit cap C_2^0 (aF)	720	675	–	410	130	240	785	685
Unit cap C_1^0 (aF)	870	780	15	440	240	350	960	770

Fig. 7 Block diagram of the self-clocking ring-oscillator loop in the ADC [6, 30]
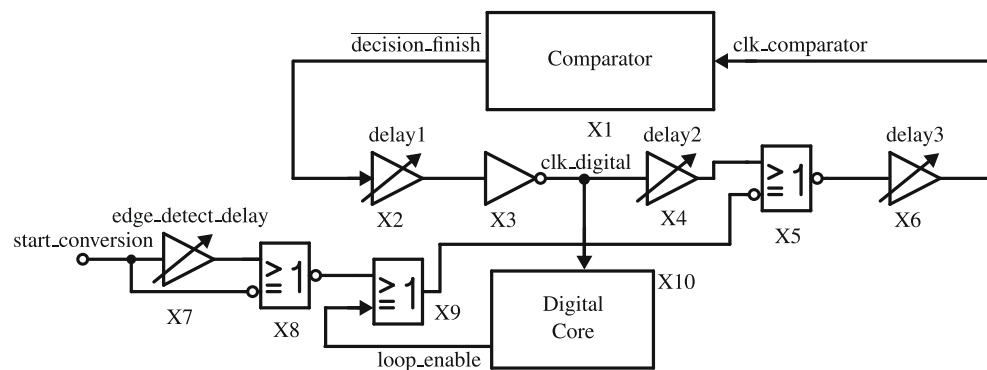
parasitics. The mismatch in the binary capacitor cells of setup c is the highest, resulting in an unreasonable use of binary-coded DAC cells. The matching in the binary cells of structure d is the best, but the gain error is increased due to additional parasitic capacitance from the top plate to the shield.

Structures e and f are no candidates for this design since the small unit capacitors show high variance. The structure g shows slightly more capacitance density than a or b, but in addition, the variance in the binary caps is also high. The last structure h shows a possible option with reasonable size and matching. As a result, the waffle capacitors of structures a and b were selected as the best topology for the proposed SAR-ADC. The result is a DAC capacitor cell with 8 unit capacitors using a waffle structure and minimum unit capacitance $C^0 = 447\,\mathrm{aF}$.

3.1.3 Semi-differential charge compensation
The capacitor is top-plate sampled, as a result, the top layer of the capacitor is critical for matching and parasitics. On the other hand, the capacitor bottom plate's potential is well-defined in this topology, parasitic capacitance to the bottom plate does not affect matching. Parasitic capacitance to the capacitor top plate can add or pull charge from the DAC capacitor. Constant parasitics to the capacitor top-plate, e.g., to V_{DD} or V_{SS}, add gain error which can be easily compensated. Parasitics to dynamic analog or digital signals add errors that cannot easily be corrected. An additional shielding layer between the capacitor bottom-plate m2 and the decoder routing layer m1 would be highly preferable to shield parasitic capacitance between the top plate and the dynamic decoder control signals. Still, the lack of available routing layers does not allow adding such a layer in this configuration.

However, simulations have shown that the gaps between the DAC capacitor cell layouts, in the assembled 12-bit DAC matrix, expose the top plate to a critical amount of parasitic capacitance, and it is necessary to compensate for this capacitance. Semi-differential[2]

---

[2] Differential layout and wiring, but single-ended evaluation of the signals.

wiring of the row and column control wires was introduced in the layout. The active-low column control signal $\overline{\mathtt{col}}$ has been extended by the active-high signal col. The row control signals $\overline{\mathtt{row}}$ and $\overline{\mathtt{rowon}}$ have been extended by signal $\overline{\mathtt{rowoff}}$ with the limitation that exactly one signal is at potential $0\,\mathrm{V}$ (active). In contrast, the other two signals must be set to $1.8\,\mathrm{V}$ (inactive).

Parasitic extraction with Magic has been used to match the parasitic capacitance between each control signal and the DAC capacitor top plate. If a control signal changes its state, the injected charge is moved to the semi-differential wire instead, and the net charge injection on the capacitor top plate is compensated. This adds complexity to the layout and the digital logic, and this compromise increases the total parasitic capacitance to the capacitor top plate; however, the initially dynamic error is shifted into the gain error.

3.1.4 Complementary sample signal generation
The row and column control signals are logically evaluated as single-ended signals, however, the pass gates in the decoder circuit as seen in Fig. 6 are driven by the differential signals sample_dac and $\overline{\mathtt{sample\_dac}}$. The complementary pass gates are sensitive to asymmetric switching of the control signals: If a state transition of the signals sample_dac and $\overline{\mathtt{sample\_dac}}$ are not symmetric, then V_{CM} and vdrv can be shorted, which negatively influences the voltage of V_{CM}.

Post-layout simulation has revealed that asymmetric switching is present if the complementary signals are generated in the digital domain; hence, a redesigned signal generation has been implemented in the analog domain. The preferred solution for future designs would be a non-overlapping clock generator for both pass gates to prevent simultaneous on-states of the gates. However, to avoid the routing overhead of additional lines, the complementary sample signal generator shown in Fig. 6 has been implemented in the DAC matrix rows to generate moderately symmetric complementary sample signals [28]. Generating an inverted signal using a single inverter adds the signal transition time of the inverter to the inverted signal, therefore, the complementary signal transitions are

Fig. 8 Delay module (automatically placed-and-routed, using a custom-made 5-ns delay cell) with the circuit of the custom delay standard cell
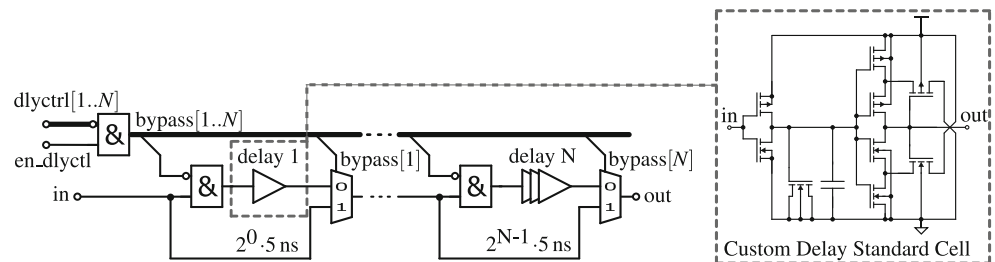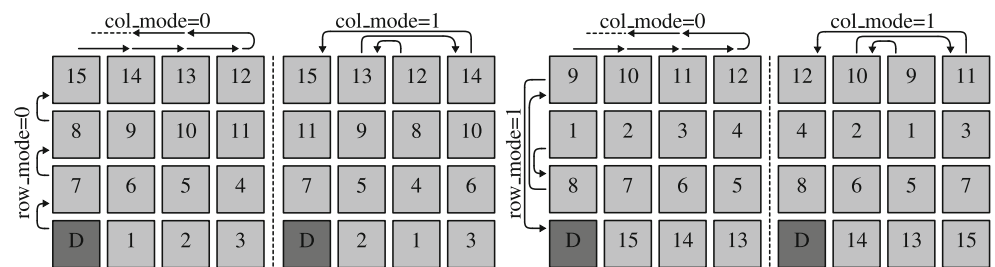

Fig. 9 The implemented DAC matrix row/column decoder modes in dependence of the configuration bit row_mode and col_mode in a 4 × 4 matrix

unsymmetrical. The implemented circuit uses the signal transition delay of a non-inverting always-on pass gate to generate a similar signal transition delay in the non-inverted signal. Both signals are then inverted again to gain similar output drivers.

3.2 Clock generator

Two clock sources are necessary for the proposed ADC, one slow clock for V_{CM} generation, and a fast clock signal `clk_digital` to control the SAR-ADC logic and the comparator. This fast clock is asynchronously generated on-chip [6] using the ring-oscillator principle, shown in Fig. 7. The clock is only active while the ADC is running to save energy.

The loop generates a clock signal with a period that corresponds to twice the transition time through three delay cells and the comparator conversion delay (the delays of the inverters and NOR gates are negligible). In this case, programmable delay cells (delay modules) are used to adjust the clock frequency to allow enough settling time for charge redistribution after switching operations and comparison. The components X7 and X8 form an edge-detect circuit to suppress multiple conversions from a single positive signal edge of the trigger signal `start_conversion`. In addition, standard cells were used as far as possible to minimize the layout effort and simplify migration to other process nodes.

As shown in Fig. 8, the delay module comprises only standard cells. Organizing the delay chains into N binary steps ($2^0 \cdot 5\,\text{ns}$, $2^1 \cdot 5\,\text{ns}$, …, $2^{N-1} \cdot 5\,\text{ns}$) allows hardware-efficient configuration using N configuration wires. AND-gates before the delay inputs are used to bypass unused delay cells and thus reduce power consumption.

The signal delay could be generated by exploiting the delay time of multiple buffers connected in series. The investigated SKY130 standard cells from the high-density (HD) library have shown a delay time in the order of 360 ps per cell. A custom delay standard cell was implemented to increase area efficiency with a delay time of 5 ns per cell. The circuit in the inset in Fig. 8 consists of a weak inverter, capacitive load, and a Schmitt-trigger circuit as the output stage. As the custom delay cell is designed using the form factor of a SKY130 digital standard cell, the layout of the delay module and the clock generator can be generated using a fully automated digital workflow using a Verilog gate-level description.

3.3 Digital control

The digital core module includes the DAC matrix row and column decoders, synchronous digital core logic, and asynchronous oversampling logic. The row and column decoder translates the current DAC code to the matrix row and column wire control signals [16]. It allows the selection of a meander or common-centroid activation style[3], the implemented modes of operation can be seen in Fig. 9. The synchronous logic handles the non-binary SAR algorithm [14] with a non-binary ratio of 1.65, clock loop control, and the calculation of the 12-bit result with averaging of the four least significant SAR weights. The oversampling module, which is asynchronously clocked using a strobe signal, calculates the 16-bit oversampled result [17].

The non-binary SAR algorithm in [22] was adapted for a fully differential SAR-ADC. M is the resolution in bit, $\Theta[k] \in \mathbb{N}$ is the kth weight of N weights while N is

---

[3] In contrast to a hand-designed full-custom row-column-decoder, accommodating different cell activation schemes is low effort when synthesizing the decoder from RTL and using an RTL-to-GDS flow for implementation.
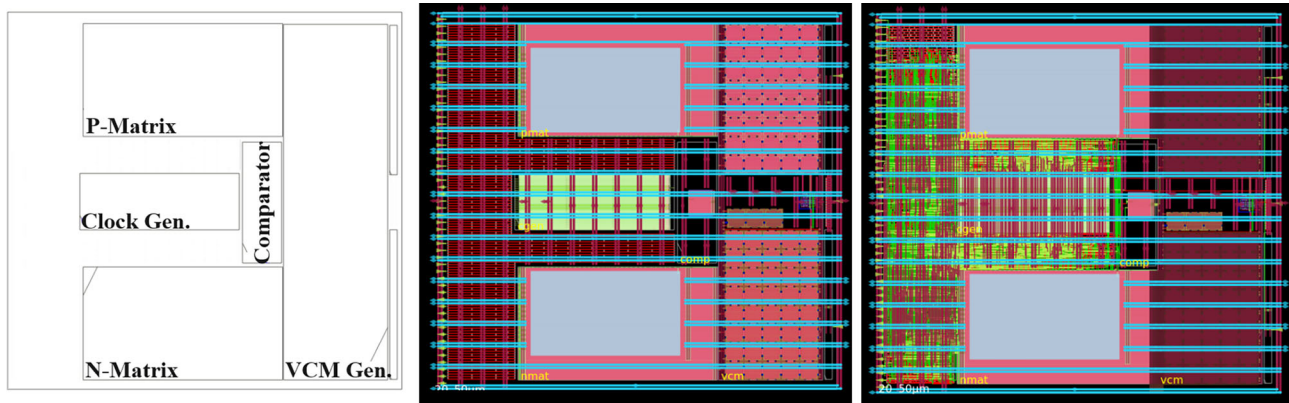
Fig. 10 Layout exploration using OpenROAD. Figure *left* to *right*: manual macro placement; power distribution network and standard cell power grid included; routing included

limited to $\{N \in \mathbb{N}_0 : N \geq M\}$, and $s[k]$ is the kth comparison result with the following conditional value:

$$s[k] = \begin{cases} +1, & \text{if } V_{\text{ctop,p}}[k] - V_{\text{ctop,n}}[k] > 0 \\ -1, & \text{otherwise} \end{cases} \quad (1)$$

$$V_{\text{ctop,p}}[k] = V_{\text{ctop,p}}[0] + V_{\text{DAC+}}[k] - V_{CM} \quad (2)$$

$$V_{\text{ctop,n}}[k] = V_{\text{ctop,n}}[0] + V_{\text{DAC−}}[k] - V_{CM} \quad (3)$$

The binary DAC value $d_{\text{DAC}\pm}[k]$ determines the analog DAC reference voltage $V_{\text{DAC}\pm}[k]$ at the kth step:

$$d_{\text{DAC}\pm}[k] = 2^{M-1} \mp \sum_{i=2}^{k} s[i-1] \cdot \Theta[i] \quad (4)$$

The chosen DAC weights $\Theta[i]$ are {2048, 806, 486, 295, 180, 110, 67, 41, 25, 15, 9, 6, 4, 2, 1} with $\sum \Theta[i] = 2^M - 1$ for $M = 12$. The result d for the non-binary M-bit SAR-ADC using N weights is in the set $\{d \in \mathbb{N}_0 : 0 \leq d \leq 2^M - 1\}$ and is calculated using the generalized formula:

$$d = 2^{M-1} + \sum_{i=2}^{N} s[i-1] \cdot \Theta[i] + \frac{1}{2}(s[N] - 1) \quad (5)$$

3.4 Top-level hardening

As seen in Fig. 2, the separated analog and digital building blocks must be combined in a top-level cell. The current OpenLane chip integration documentation [23] specifies a macro hardening stage, integration of hardened macros into the chip core, and integration of the hardened core into the pad frame. Each hierarchical level reduces the highest allowed metal layer by one level in such a hierarchical design. In the chip core level, metal layer m5 is used for the PDN to connect macros to their power rails on m4. However, a macro inside another macro would be limited to the usage of m3 as the highest layer, and so on.

This limitation had to be overruled in this work because SKY130 MIMCAP layers use m4 at the lowest hierarchy. According to the documentation, the integration of a macro with MIMCAP layers, as seen

in the comparator and V_{CM} generator, must be done in the OpenLane core hierarchy. A method has been found to integrate macros at the same hierarchical metal layer as the current PDN generation. The ADC hard-macro IP is hardened as a chip-core using metal layers up to m5 in a way that allows integration into another chip core at metal layer m5. However, if done correctly, this method violates the documented rules for chip integration, not the process's design rules. The PDN generator has been found to avoid short circuits and connect macros to the PDN if PORT layers in the LEF file at the PDN metal layers m4-5 are also defined in the FP_PDN_MACRO_HOOKS configuration of OpenLane, all other nets specified in the LEF file at the PDN layers must be protected by obstruction OBS layers. For example, these obstruction layers have been used in the DAC matrix to prevent the generation of m5 structures above the DAC top plate capacitor. The hardened SAR-ADC macro is surrounded by a core ring, which allows power connections of the SAR-ADC to the top-level power network at the edge of the IP block.

OpenLane has been configured to generate the SAR-ADC top-level hard-macro IP using a digital-on-top workflow, the different hardening stages are shown in Fig. 10 using OpenROAD. The workflow utilizes the GDSII and LEF file format as input for the custom analog macro cells (DAC, comparator, V_{CM} generator, clock generator), and the digital RTL is synthesized, as is shown in Fig. 1. The macros are placed on the top-level macro area by manually specified coordinates at fixed core dimensions. The digital standard cell grid is generated around the placed macros on unused space. The analog macros and the digital standard cell grid are connected to the generated PDN on m4 and m5. This work uses a vertical m4 and horizontal m5 PDN. For the clock generator, a custom PDN generation Tcl script was used to allow connection from m4 down to m3, since the power rails of the clock generator have been placed on level m3. After PDN generation, the clock tree is synthesized, standard cells are placed on the standard cell

Fig. 11 DAC matrix transfer curves of the pre-layout and post-layout simulation (the data vector sweeps from value 0 to 4095). **a** shows the full transfer curve, **b** is zoomed to DAC code 2048, showing the mismatch in the LSB bit translation
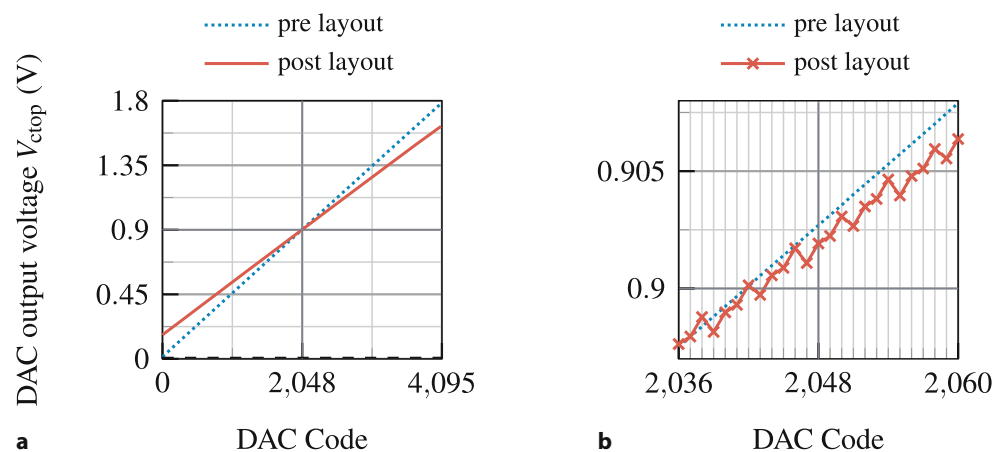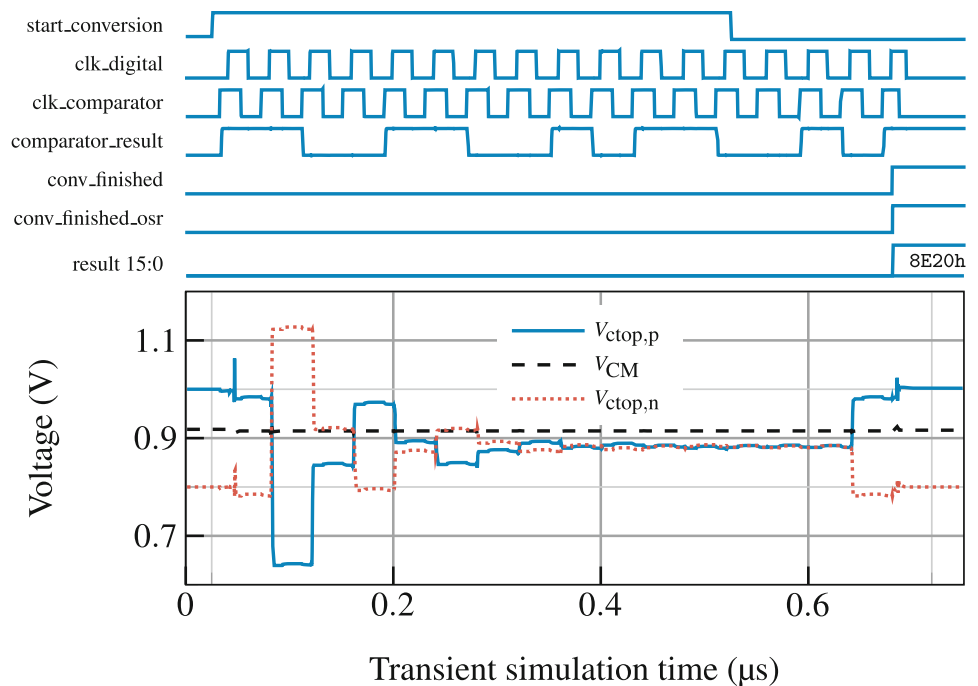

Fig. 12 Post-layout simulation of an A/D conversion at the fastest configuration f_s = 1/694 ns = 1.44 MS/s. The differential voltage $V_{inp} - V_{inn}$ has been set to 200 mV. The conversion has been triggered after power-up and settling of the generated common mode voltage V_{CM}

grid, and routing is performed. After several rounds of optimization, the flow is completed, and the top-level GDS and LEF are generated. Since the OpenLane workflow was initially intended for digital workflows, the layout is optimized manually using KLayout for cleaner and wider analog signal routes.

4 Simulation results

The transfer function of the assembled DAC before and after post-layout parasitic C-extraction using Magic is shown in Fig. 11. The simulator ngspice has been used to run the simulation. Fig. 11a shows the inherently good linearity of the capacitive charge-redistribution DAC topology, but the full-scale range is limited to 0.167–1.672 V due to gain- and offset-errors. The zoomed DAC transfer function in Fig. 11b shows the mismatch in the LSB bits. The top-level post-layout SPICE netlist has been generated using

the parasitic C-extraction from the VLSI layout tool Magic with the configuration ext2spice cthresh 0.1. The resulting netlist contains 26e3 MOSFETs and 60e3 capacitors. The schematic tool Xschem has been used to build a test environment with disabled averaging, no oversampling, and the fastest clock frequency. The A/D conversion has been simulated using the parallel simulator Xyce at precision settings ABSTOL=1E-15 and RELTOL=1E-6. Although Monte Carlo mismatch simulations are possible by using the presented open-source tools, they could not be performed for the proposed SAR-ADC since the design is far too big, leading to a very long simulation time for a reasonable set of data points. However, the proposed SAR-ADC was proven by corner simulations. The plot in Fig. 12 shows a conversion time of T_{conv} = 694 ns which corresponds to a sample rate of f_s = 1.44 MS/s at an average power consumption of 703 μW. Table 3 shows the comparable performance

Table 3 Comparison to similar SAR-ADCs

References	ASSCC	ASSCC	CICC	ICECS	GitHub	This work
	[32]'19	[43]'19	[4]'19	[31]'20	[3]'23	
Process (nm)	180	65	65	180	130	130
Open-source	no	no	no	no	yes	**yes**
Supply (V)	1.5	1.0	1.2	1.0	1.8	1.8
Resolution (bit)	12	9	10	14	10	12
OSR	8	8	1	4	1	1
Sample rate (kHz)	5120	10000	4000	4.096	1560	1440
Power (µW)	180.1	130	149	1.125	2100	703
Area (mm^2)	0.192	0.072	0.24	0.349	0.149	0.175
FoM$_W$ (fJ/step)	180.7	35.9	87.7	158.2	2.12K	281†
FoM$_S$ (dB)	158.1	167.8	155.6	165.2	113.5	156.6†

$\text{FoM}_W = P/(2^{(\text{SNDR}-1.76)/6.02} \cdot 2\text{BW})$, $\text{FoM}_S = \text{SNDR} + 10\log(\text{BW}/P)$ † As this work is similar to [31], $\text{SNDR} = 66.5\,\text{dB}$ is assumed for FoM estimation.

of this open-source SAR-ADC to the state-of-the-art, designed with commercial tools.

5 Conclusion

A 12-bit SAR-ADC has been designed (using only open-source EDA tools) for the open-source SKY130 technology. It is highly configurable and features integrated decimation filters to increase the output word size up to 16 Bit. The integrated clock generator is hardened using a digital design workflow by extending it with custom-made cells. A production-ready layout (shown in Fig. 13, including an overlay indicating main blocks) has been generated with a digital-on-top design flow, integrating the synthesized RTL of the digital control block with custom analog layouts of the DAC, comparator, and V_{CM} generator, next to the automatically hardened clock generator.
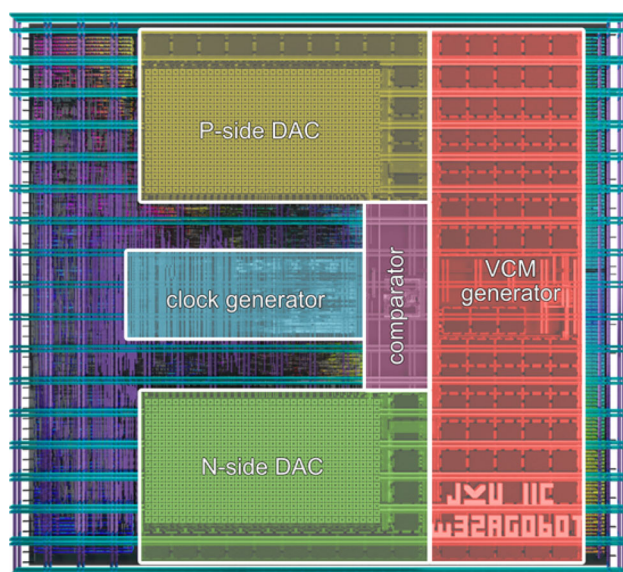

Fig. 13 Floor plan of the proposed 12-bit SAR-ADC layout (434 µm × 403 µm). The 3D visualization has been created using gdsiistl [13] and Blender [5]

The simulated performance of this ADC is comparable to similar SAR-ADCs that have been designed with commercial tools and demonstrates the progress that free and open-source integrated circuit design tools have made recently.

References

1. Ajayi T, Blaauw D, Chan TB, Cheng CK, Chhabria V, Choo DK, Coltella M, Dreslinski RG, Fogaça M, Hashemi SM, Ibrahim AA, Kahng AB, Kim M, Li J, Liang Z, Mallappa U, Pénzes PI, Pradipta G, Reda S, Rovinski A, Samadi K, Sapatnekar SS, Saul LK, Sechen C, Srinivas V, Swartz W, Sylvester D, Urquhart D, Wang L, Woo M, Xu B (2019) OpenROAD: Toward a self-driving, open-source digital layout implementation tool chain. In: Archive University of Minnesota. https://api.semanticscholar.org/CorpusID:210937106. Accessed 15-12-2023

2. Ajayi T, Chhabria VA, Fogaça M, Hashemi S, Hosny A, Kahng AB, Kim M, Lee J, Mallappa U, Neseem M, Pradipta G, Reda S, Saligane M, Sapatnekar SS, Sechen C, Shalan M, Swartz W, Wang L, Wang Z, Woo M, Xu B (2019pp)

Toward an open-source digital flow: first learnings from the OpenROAD project. Proceedings of the 56th annual design automation. Conference, vol 2019, pp 1–4 https://doi.org/10.1145/3316781.3326334

3. Beal DA et al (2023) 10b SAR ADC developed at the University of Alabama. https://github.com/UAH-IC-Design-Team/sky130-10-bit-SAR-ADC. Accessed 15-12-2023

4. Bindra HS, Annema AJ, Wienk G, Nauta B, Louwsma SM (2019) A 4MS/s 10b SAR ADC with integrated Class-A buffers in 65nm CMOS with near rail-to-rail input using a single 1.2 V supply. In: IEEE Custom Integrated Circuits Conference, pp 1–4 https://doi.org/10.1109/CICC.2019.8780150

5. Blender – free and open 3D creation software. https://www.blender.org. Accessed 20-09-2023

6. Chen SWM, Brodersen RW (2006) A 6-bit 600-MS/s 5.3-mW asynchronous ADC in 0.13-µm CMOS. IEEE J Solid-State Circuits 41(12):2669–2680. https://doi.org/10.1109/JSSC.2006.884231

7. Clark LT, Vashishtha V, Shifren L, Gujja A, Sinha S, Cline B, Ramamurthy C, Yeric G (2016) ASAP7: A 7-nm finFET predictive process design kit. Microelectronics J 53:105–115. https://doi.org/10.1016/j.mejo.2016.04.006

8. Docker website. https://www.docker.com. Accessed 26-09-2023

9. Edwards RT Magic VLSI layout tool. https://github.com/rtimothyedwards/magic. Accessed 19-09-2023

10. Edwards RT Netgen complete LVS tool for comparing SPICE or Verilog netlists. https://github.com/rtimothyedwards/netgen. Accessed 19-09-2023

11. Edwards RT, Shalan M, Kassem M (2021) Real silicon using open-source EDA. IEEE Des Test 38(2):38–44. https://doi.org/10.1109/mdat.2021.3050000

12. van Elzakker M, van Tuijl E, Geraedts P, Schinkel D, Klumperink E, Nauta B (2008) A 1.9 µW 4.4 fJ/conversion-step 10b 1MS/s charge-redistribution ADC. In: IEEE International Solid-State Circuits Conference – Digest of Technical Papers, pp 244–610 https://doi.org/10.1109/ISSCC.2008.4523148

13. gdsiistl: Converts GDSII files to STL files. https://github.com/andrsmllr/gdsiistl. Accessed 20-09-2023

14. Kuttner F (2002) A 1.2V 10b 20MSample/s non-binary successive approximation ADC in 0.13µm CMOS. In: IEEE International Solid-State Circuits Conference. Digest of Technical Papers (Cat. No.02CH37315), vol 1, pp 176–177 https://doi.org/10.1109/ISSCC.2002.992993

15. Köfferlein M KLayout. https://github.com/KLayout/klayout. Accessed 19-09-2023

16. Miki T, Nakamura Y, Nakaya M, Asai S, Akasaka Y, Horiba Y (1986) An 80-MHz 8-bit CMOS D/A converter. IEEE J Solid-State Circuits 21(6):983–988. https://doi.org/10.1109/JSSC.1986.1052639

17. Moser M (2023) Design of a low-power 12-bit non-binary charge-redistribution SAR-ADC utilizing the SKY130 open-source technology. https://epub.jku.at/urn/urn:nbn:at:at-ubl:1-62352. Accessed 15-12-2023

18. Moser M (2023) GitHub repository of the SKY130 SAR-ADC. https://github.com/iic-jku/SKY130_SAR-ADC1. Accessed 15-12-2023

19. Moser M, Fath P, Zachl G, Pretl H (2023) An open-source 1.44-MS/s 703-µW 12-bit non-binary SAR-ADC using 448-aF capacitors in 130-nm CMOS. In: Austrochip Workshop on Microelectronics (Austrochip), pp 2–5 https://doi.org/10.1109/Austrochip61217.2023.10285152

20. Nagel LW, Pederson D (1973) SPICE (simulation program with integrated circuit emphasis). Tech. Rep. UCB/ERL M382, EECS Department, University of California, Berkeley. http://www2.eecs.berkeley.edu/Pubs/TechRpts/1973/22871.html. Accessed 15-12-2023

21. ngspice. https://ngspice.sourceforge.io. Accessed 19-09-2023

22. Ogawa T, Matsuura T, Kobayashi H, Takai N, Hotta M, San H, Abe A, Yagi K, Mori T (2010) Non-binary SAR ADC with digital error correction for low power applications. In: IEEE Asia Pacific Conference on Circuits and Systems, vol 2010, pp 196–199 https://doi.org/10.1109/APCCAS.2010.5774747

23. OpenLane. https://github.com/The-OpenROAD-Project/OpenLane. Accessed 19-09-2023

24. The-OpenROAD-Project. https://github.com/The-OpenROAD-Project/OpenROAD. Accessed 19-09-2023

25. Ousterhout J, Hamachi G, Mayo R, Scott W, Taylor G (1984) Magic: A VLSI layout system. In: 21st Design Automation Conference Proceedings, pp 152–159 https://doi.org/10.1109/DAC.1984.1585789

26. Pretl H JKU IIC OSIC-Multitool for open-source IC design for SKY130. https://github.com/iic-jku/osic-multitool. Accessed 19-09-2023

27. Pretl H, Zachl G (2023) GitHub repository of the IIC OSIC TOOLS. https://github.com/iic-jku/IIC-OSIC-TOOLS. Accessed 15-12-2023

28. Razavi B (2016) Design of Analog CMOS IC, 2nd edn. McGraw-Hill

29. Schippers S Xschem. https://github.com/StefanSchippers/xschem. Accessed 19-09-2023

30. Schmickl S (2021) Design methodology and development of battery-less SoCs for bio-sensing. https://epub.jku.at/urn:nbn:at:at-ubl:1-43787. Accessed 15-12-2023

31. Schmickl S, Faseth T, Pretl H (2020) An untrimmed 14-bit non-binary SAR-ADC using 0.37 fF-capacitors in 180 nm for 1.1 µW at 4 kS/s. In: 27th IEEE international conference on electronics, circuits and systems (ICECS), pp 1–4 https://doi.org/10.1109/ICECS49266.2020.9294971

32. Seo MJ, Jin DH, Kim YD, Kim JP, Chang DJ, Lim WM, Chung JH, Park CU, An EJ, Ryu ST (2019) A single-supply buffer-embedding SAR ADC with skip-reset having inherent chopping capability. In: IEEE Asian Solid-State Circuits Conference (A-SSCC), pp 189–192 https://doi.org/10.1109/A-SSCC47793.2019.9056894

33. Shalan M, Edwards T (2020) Building OpenLANE: A 130nm OpenROAD-based tapeout-proven flow: Invited paper. In: IEEE/ACM International Conference On Computer Aided Design (ICCAD), pp 1–6

34. Open source process design kit for usage with SkyWater Technology Foundry's 130nm node. https://github.com/google/skywater-pdk. Accessed 19-09-2023

35. SkyWater SKY130 PDK 0.0.0-369-g7198cf6 documentation. https://skywater-pdk.readthedocs.io/en/main/index.html. Accessed 20-09-2023

36. Snyder W Verilator open-source systemverilog simulator and lint system. https://github.com/verilator/verilator. Accessed 19-09-2023

37. Suarez R, Gray P, Hodges D (1975) All-MOS charge redistribution analog-to-digital conversion techniques. I. IEEE J Solid-State Circuits 10(6):379–385. https://doi.org/10.1109/JSSC.1975.1050630

38. Williams S Icarus Verilog. https://github.com/steveicarus/iverilog. Accessed 19-09-2023

39. Wolf C Yosys open synthesis suite. https://github.com/YosysHQ/yosys. Accessed 19-09-2023

40. Wolf C, Glaser J (2013) Yosys – a free Verilog synthesis suite. https://api.semanticscholar.org/CorpusID:202611483. Accessed 15-12-2023

41. Xie Y, Ansell T, Saligane M (2020) The missing pieces of open design enablement. Proceedings of the 39th International

Conference on Computer-Aided Design, pp 1–8 https://doi.org/10.1145/3400302.3415736

42. The Xyce™ Parallel Electronic Simulator. https://github.com/Xyce/Xyce. Accessed 19-09-2023

43. Yoon JS, Hong J, Kim J (2019) A digitally-calibrated 70.98dB-SNDR 625kHz-bandwidth temperature-tolerant 2nd-order noise-shaping SAR ADC in 65nm CMOS. In: IEEE Asian Solid-State Circuits Conference (A-SSCC), pp 195–196 https://doi.org/10.1109/A-SSCC47793.2019.9056963

Publisher's Note Springer Nature remains neutral with regard to jurisdictional claims in published maps and institutional affiliations.

Patrick Fath, was born in Vöcklabruck, Austria, in 1992. He received his B.Sc. and M.Sc. degrees in Mechatronics from Johannes Kepler University Linz in 2017 and 2020. In addition, he received B.Sc. and M.Sc. degrees in Electronics and Information Technology from the JKU in 2018 and 2021. His first master's thesis addressed the design of a passive 180nm receiver-front-end for low-power SRD applications and his second addressed the design of an RX-topology for a 7-GHz UWB communication system. In April 2021 he joined the Institute for Integrated Circuits (IIC) at the Johannes Kepler University Linz working towards his Ph.D. degree. His current research focuses on a wireless 1024-channel biosignal acquisition system and open-source chip design. He is recipient of the best paper award at the 2023 IEEE Nordic Circuits and Systems Conference.

Manuel Moser, was born in Salzburg, Austria, in 1991. He received his Dipl.-Ing. degree in Electronics and Information Technology from Johannes Kepler University Linz in 2023. His master's thesis addressed the design of a low-power 12-bit SAR-ADC utilizing the SKY130 Open-Source technology.

Georg Zachl, was born in Steyr, Austria in 1993. He received his B.Sc. and M.Sc. degrees in Electronics and Information Technology from Johannes Kepler University (JKU) Linz in 2018 and 2020. In his master's thesis, he worked on analyzing the near-field electromagnetic emissions of printed circuit boards using measurements and simulations. In December 2020, he joined the Institute for Integrated Circuits (IIC) at the Johannes Kepler University, where he is now pursuing a Ph.D. degree. His research focuses on mm-Wave / sub-THz TRX circuits and open-source chip design.

Harald Pretl, (S'97-M'01-SM'08) received a Dipl.-Ing. degree (with distinction) in electrical engineering from the Graz University of Technology, Austria, in 1997, and the Dr. techn. degree from the Johannes Kepler University (JKU) in Linz, Austria, in 2001, for his work on first-generation direct-conversion transceivers for UMTS (3G). From 2000 to 2011 he worked at Infineon Technologies as Director and Senior Principal Engineer, from 2011 to 2019 at Intel as Senior Principal Engineer and Chief RF Technologist, and from 2019 to 2022 at Apple, contributing to several generations of cellular RF transceivers and mobile communications platforms, spanning from 2G to 5G, as analog circuit designer, project lead and RF systems architect. Since 2015 he has been a full professor heading the Institute for Integrated Circuits (IIC) at the JKU, Linz, where he is leading the Energy-Efficient Analog Circuits & Systems Group. Harald is a co-lead of the LIT/SAL mmWave Lab and the lead developer of the IIC-OSIC-TOOLS, an open-source IC design environment. Harald Pretl was a member of the technical program committee of the ISSCC in 2010–2012 and has published more than 90 papers at international conferences and journals in the area of RF transceivers and analog circuits, in addition to more than 25 issued or filed patents. His current research interests are focused on cellular transceivers, wireless sensor networks, micro-power RF SoC for medical applications, and mm-wave circuits for 6G and advanced radar, as well as open-source IC design. He is a co-recipient of first place in the 2015 MTT-S PAWR student paper competition, the 2019 ReSMiQ best paper award at the IEEE NEWCAS conference, the 2019 APMC student prize, a 2021 ISCAS best paper award, and the 2023 IEEE NorCAS best paper award. He is also a co-recipient of the Intel Achievement Award in 2019. He is a member of the Austrian Electrotechnical Association (OVE), the Association for Electrical, Electronic & Information Technologies (VDE), and the IEEE SSCS Technical Committee on the Open Source Ecosystem (TC-OSE).